J. Fluid Mech. (1995), *vol.* 294, *pp.* 231–257

Unicellular natural circulation in a shallow horizontal porous layer heated from below by a constant flux

By S. KIMURA[1],† M. VYNNYCKY[1] AND F. ALAVYOON[2]

[1] Tohoku National Industrial Research Institute, Agency of Industrial Science and Technology, Ministry of International Trade and Industry, 4-2-1 Nigatake, Miyagino-Ku, Sendai, 983, Japan

[2] Vattenfall Utveckling AB, S-810 70 Älvkarleby, Sweden

(Received 22 March 1994 and in revised form 23 January 1995)

Natural convection in a saturated horizontal porous layer heated from below and cooled at the top with a constant flux is studied both analytically and numerically. Linear stability analysis indicates that unicellular recirculation remains a stable mode of flow as the aspect ratio (A) of the layer is increased, in contrast to the situation for an isothermally heated and cooled layer. An analytical solution is presented for fully developed counterflow in the infinite-aspect-ratio limit; this flow is found to be linearly stable to transverse disturbances for Rayleigh number (Ra) as high as 506, at which point a Hopf bifurcation sets in; however, further analysis indicates that an exchange of stability due to longitudinal disturbances will occur much sooner at $Ra \approx 311.53$. The velocity and temperature profiles of the counterflow solution, whilst not strictly speaking valid in the extreme end regions of the layer, otherwise agree very well with full numerical computations conducted for the ranges $25 \leqslant Ra \leqslant 1050$, $2 \leqslant A \leqslant 10$. However, for sufficiently high Rayleigh number (Ra between 630 and 650 for $A = 8$ and Ra between 730 and 750 for $A = 4$, for example), the computations indicate transition from steady unicellular to oscillatory flow, in line with the Hopf bifurcation predicted by the linear stability analysis for infinite aspect ratio.

1. Introduction

Convection in a two-dimensional rectangular fluid-saturated porous medium heated from below may take various flow patterns depending on the imposed thermal boundary conditions. For conventional boundary conditions, that is isothermal horizontal and adiabatic side walls and commonly known as Lapwood convection, it has been established that, in a domain of unit aspect ratio, a single-cell solution undergoes a series of bifurcations as the Rayleigh number is increased. A Hopf bifurcation has been observed for two-dimensional single-cell convection by, for instance, Horne & O'Sullivan (1974), Caltagirone (1975), Schubert & Straus (1982) and Gary & Kassoy (1981); the definitive value of the critical Rayleigh number for a square cavity, however, has been determined recently as $Ra = 390$ (Kimura, Schubert & Straus 1986, 1987; Aidun & Steen 1987). A thorough picture of the bifurcation process for multicellular flows within two-dimensional cavities, involving a detailed account of the dependency on cavity aspect ratio, was presented by Riley & Winters

† Present address: Department of Mechanical Engineering, Kanazawa University 2-40-20 Kodatsumo, Kanazawa, 920, Japan.

(1989, 1991); in particular, their results indicate that single-cell flow is the leading primary solution when the aspect ratio is less than $\sqrt{2}$, with multicellular flow being the preferred mode for aspect ratios greater than this value.

Extensions of the problem to three dimensions, assuming the four sidewalls to be adiabatic, have been made by Schubert & Strauss (1979), Steen (1983) and Kimura *et al.* (1989). This adiabatic condition, while being one of the simplest, may not, in many practical situations, be appropriate: for example, in the modelling of convective heat flow within a fault zone in the Earth's crust, where the heat exchange through the vertical confining boundaries cannot be neglected. The sidewall heat loss on the broader sides and its influence on the onset of convection was first studied by Lowell & Shyu (1978) and Murphy (1979); their results indicate that, when sidewall heat loss is permitted, the critical Rayleigh number for the onset of convection becomes significantly greater than $4\pi^2$. More complete analyses have been presented in a series of papers by Kassoy & Cotte (1985), Weidman & Kassoy (1986) and Wang, Kassoy & Weidman (1987), where the critical Rayleigh number and the modal configuration for convection were found to be extremely sensitive to the sidewall thermal conditions. Supercritical states for this problem have yet to be investigated, however.

As far as the heating condition on the horizontal wall is concerned, on the other hand, one simple alternative to constant temperature would be a condition of constant flux. This condition, although it seems only realizable by means of a carefully arranged experiment, may be readily obtained when a slab of finite thermal conductivity is present between a constant-temperature surface and the slab–porous boundary (Kimura & Pop 1992). This implies that the constant-flux condition may arise more frequently in real life than does the constant-temperature one: for example, in the electrochemical systems considered by Bark, Alavyoon & Dahlkild (1992) and Alavyoon (1992). It was first found by Bejan (1983) that when a constant heat flux is specified along the vertical boundaries of a tall rectangular cavity, the flow, unlike that for the constant-temperature case, has a strikingly simple structure: namely, thermal and velocity boundary layers of constant thickness, with core and boundary temperatures increasing linearly in the upward direction.

Vasseur, Satish & Robillard (1987) and Sen, Vasseur & Robillard (1987) analysed unicellular natural convection in an inclined shallow porous layer when the two facing walls are subject to a constant flux (one for heating and the other for cooling). Focusing on the mid-portion of the layer, they were able to develop an analytical solution for the temperature and the streamfunction for an arbitrary angle of inclination with respect to gravitational acceleration. Two-dimensional numerical results were also presented to test the closed-form solutions; the validity of the analytical solution was thus verified. One of their main points of interest centres on the question as to whether unicellular convection is stable within a small angle of inclination from the horizontal position, since it is evident that a vertical temperature gradient may break up a unicellular flow into multiple cells. With regard to this question, they found numerically that unicellular flow is in fact stable at small angles of inclination, and that within a horizontal layer a unicellular flow may stably exist up to a finite supercritical Rayleigh number, despite the presence of a mechanism to drive the flow upward at any horizontal position. However, they did not comment explicitly on, nor investigate, the possible stability of unicellular convection in the horizontal layer. Therefore, it is not yet clear whether the unicellular flow is *the only stable* convective pattern in the supercritical state, if so up to what value of the Rayleigh number the unicellular flow can stably exist, and furthermore what alternative state eventually replaces the steady unicellular flow if the Rayleigh number exceeds the

second criticality. In other words, the question remains as to whether or not the surprisingly simple flow structure envisaged by Bejan (1983) for the side-heating problem in a vertical layer would also persist in a horizontal layer heated from below.

Our general preconceptual view of convection in a shallow layer heated from below is the formation of a number of convecting cells whose width is roughly that of the layer height. Stable unicellular convection in a shallow layer may drastically alter this picture of convecting patterns. At this point it would be worth mentioning that in one particular case, that of a shallow horizontal layer subjected to an inclined temperature gradient (Weber 1974), a unicellular flow does in fact exist. Nield (1991) has recently made a stability analysis of this problem for a more general parametric range which reveals several different bifurcations from the fully developed counter-flow, depending upon the ratio between the horizontal and vertical temperature gradients; the present analysis will show that such bifurcations may in fact be realized as a consequence of a much simpler boundary condition, namely heating and cooling with a constant flux. The proposed system involves fewer parameters, and is thus more amenable to the study of momentum and heat transfer characteristics. This paper will seek to demonstrate the existence of a unicellular flow when the layer is heated and cooled by constant fluxes, and to identify a possible criticality beyond which a steady state no longer exists, the transition from steady to oscillatory state occurring in the same manner as for constant-temperature boundary conditions.

In what follows, we first define a physical model and present a mathematical formulation to describe the problem in §2. In §3, we consider first the linear stability of the conductive state for arbitrary aspect ratio, and then derive an analytical solution for the flow and temperature fields, which is valid in a fully developed flow regime for infinite aspect ratio. Subsequently, a normal mode linear stability analysis, both in two and three dimensions, is conducted in order to demonstrate and to enforce our argument that unicellular convection can exist at a finite supercritical Rayleigh number for infinite aspect ratio. In §4 we integrate the full governing equations numerically to see the effect of finite aspect ratio. Finally, concluding remarks are made in §5.

2. Mathematical formulation

Before we describe our mathematical formulation, the basic assumptions underlying the present work are reviewed. First we assume that the solid matrix is homogeneous, isotropic and non-deformable with respect to the saturating fluid. The flow in a porous medium is described by a linear Darcy law; the Darcy number is small, so that the inertia terms can be neglected. The magnitude of the velocity is small and the solid matrix and the fluid are in thermal equilibrium. The relative temperatures across the layer are also small so that the Boussinesq approximation is valid.

We consider a shallow cavity as shown in figure 1; the aspect ratio $A = W/H$, where W is the width of the cavity and H is the height, is assumed to be large but finite, although the cavity is assumed to be of infinite extent in the z-direction. The space is filled with a porous matrix of porosity ϕ, permeability K and thermal capacity $(\rho C)_s$, and saturated by a fluid whose kinematic viscosity, thermal expansion coefficient and thermal capacity are ν, β and $(\rho C)_f$ respectively. It is assumed that the fluid-saturated porous medium is characterized by an effective thermal conductivity k_e, an effective thermal capacity $(\rho C)_e$ defined by $\phi(\rho C)_f+(1-\phi)(\rho C)_s$, and a thermal diffusivity α defined by $k_e/(\rho C)_f$.

The top and bottom horizontal boundaries are subject to constant heat fluxes, which, respectively, cool and heat at the same rate. The two sidewalls are thermally

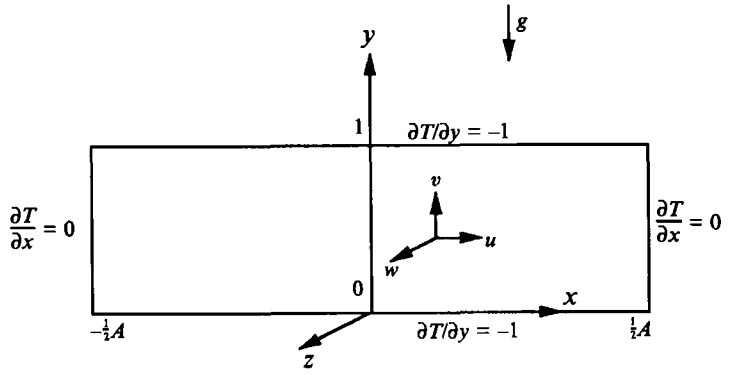

FIGURE 1. Physical model and coordinate system for a horizontal rectangular cavity heated from below by a constant flux.

insulated and all boundaries are taken to be impermeable to the saturating fluid. Upon invoking the Boussinesq approximation and the linear Darcy law, the non-dimensional equations for the convective flow are

$$\nabla \cdot \boldsymbol{q} = 0, \tag{1}$$

$$\nabla p + \boldsymbol{q} - Ra T \boldsymbol{j} = 0, \tag{2}$$

$$\partial T/\partial t + \boldsymbol{q} \cdot \nabla T - \nabla^2 T = 0, \tag{3}$$

where $\boldsymbol{q}$ is the velocity vector, $\boldsymbol{j}$ is the unit vector in the vertical direction, T is the temperature and p is the pressure. In addition, the non-dimensionalization has been performed in accordance with

$$(x, y, z) = \frac{(x^*, y^*, z^*)}{H}, \quad \boldsymbol{q} = \frac{\boldsymbol{q}^*}{\alpha/H}, \quad T = \frac{T^*}{Q'' H/k_e}, \quad p = \frac{p^*}{\mu\alpha/K}, \quad t = \frac{t^*}{\gamma H^2/\alpha}. \tag{4}$$

where Q'' is a constant heat flux specified along the horizontal boundaries, γ is the thermal capacity ratio of the porous medium defined by

$$\gamma = (\phi(\rho C)_f + (1-\phi)(\rho C)_s)/(\rho C)_f$$

and the Rayleigh number is given by

$$Ra = \frac{g\beta K Q'' H^2}{\alpha \nu k_e}, \tag{5}$$

with K as the permeability of the porous medium. The boundary conditions are written as

$$u = 0, \quad \partial T/\partial x = 0 \quad \text{on} \quad x = \pm A/2, \tag{6}$$

$$v = 0, \quad \partial T/\partial y = -1 \quad \text{on} \quad y = 0, 1, \tag{7}$$

where the components of $\boldsymbol{q}$ are (u, v, w).

3. Theoretical considerations

3.1. *Onset of convection*

We consider first the criticality condition for the onset of convection; this has been derived already for infinite aspect ratio by Nield (1968), and so we consider the finite

case. Since Squire's theorem holds, for linear stability it is sufficient to consider just (x, y)-disturbances on the base state

$$u_0 = v_0 = w_0 = 0, \tag{8}$$

$$T_0 = -y, \tag{9}$$

$$p_0 = -\tfrac{1}{2}Ray^2; \tag{10}$$

writing

$$(u, v) = (u_0, v_0) + (\hat{u}(x, y, t), \hat{v}(x, y, t)),$$

$$T = T_0(y) + \hat{T}(x, y, t),$$

$$p = p_0(x, y) + \hat{p}(x, y, t),$$

and assuming that the perturbation quantities (those with carets) are small, we substitute into equations (1)–(3), linearize by neglecting products of small quantities, cross-differentiate to eliminate $\hat{p}$ and introduce a streamfunction $\hat{\psi}$ given by

$$\hat{u} = \partial\hat{\psi}/\partial y, \quad \hat{v} = -\partial\hat{\psi}/\partial x,$$

to obtain

$$\nabla^2\hat{\psi} = -Ra\,\partial\hat{T}/\partial x, \tag{11}$$

$$\partial\hat{T}/\partial t - \partial\hat{\psi}/\partial x = \nabla^2\hat{T}, \tag{12}$$

subject to the homogeneous boundary conditions

$$\hat{\psi} = 0, \quad \partial\hat{T}/\partial x = 0 \quad \text{on} \quad x = \pm A/2, \tag{13}$$

$$\hat{\psi} = 0, \quad \partial\hat{T}/\partial y = 0 \quad \text{on} \quad y = 0, 1. \tag{14}$$

Taking normal mode expansions which satisfy (13), that is

$$(\hat{\psi}, \hat{T}) = \left[F(y)\sin\frac{m\pi}{A}\left(x + \frac{A}{2}\right), G(y)\cos\frac{m\pi}{A}\left(x + \frac{A}{2}\right)\right]e^{\sigma t},$$

where m is a strictly positive integer and σ is a complex number, we substitute into (11) and (12), which may then be combined to give

$$F'''' - \left(\sigma + \frac{2m^2\pi^2}{A^2}\right)F'' + \frac{m^2\pi^2}{A^2}\left(\sigma + \frac{m^2\pi^2}{A^2} - Ra\right)F = 0, \tag{15}$$

subject to (14), which becomes

$$F(0) = 0, \quad F''''(0) = \frac{m^2\pi^2}{A^2}F'(0), \tag{16}$$

$$F(1) = 0, \quad F''''(1) = \frac{m^2\pi^2}{A^2}F'(1). \tag{17}$$

To determine the eigenmodes, we set $\sigma = 0$ for neutral stability and note that if e^{iay} satisfies (15), where a is real, then so will e^{by}, provided

$$b = \left(\frac{2m^2\pi^2}{A^2} + a^2\right)^{1/2}.$$

Thence we are led to consider the eigenfunctions

$$F_{\lambda_n}(y) = \frac{\cosh(\lambda_{m,n}^2 + 2m^2\pi^2/A^2)^{1/2}(y - \frac{1}{2})}{\cosh\frac{1}{2}(\lambda_{m,n}^2 + 2m^2\pi^2/A^2)^{1/2}} - \frac{\cos\lambda_{m,n}(y - \frac{1}{2})}{\cos\frac{1}{2}\lambda_{m,n}}, \tag{18}$$

$$F_{\mu_n}(y) = \frac{\sinh(\mu_{m,n}^2 + 2m^2\pi^2/A^2)^{1/2}(y - \frac{1}{2})}{\sinh\frac{1}{2}(\mu_{m,n}^2 + 2m^2\pi^2/A^2)^{1/2}} - \frac{\sin\mu_{m,n}(y - \frac{1}{2})}{\sin\frac{1}{2}\mu_{m,n}}, \tag{19}$$

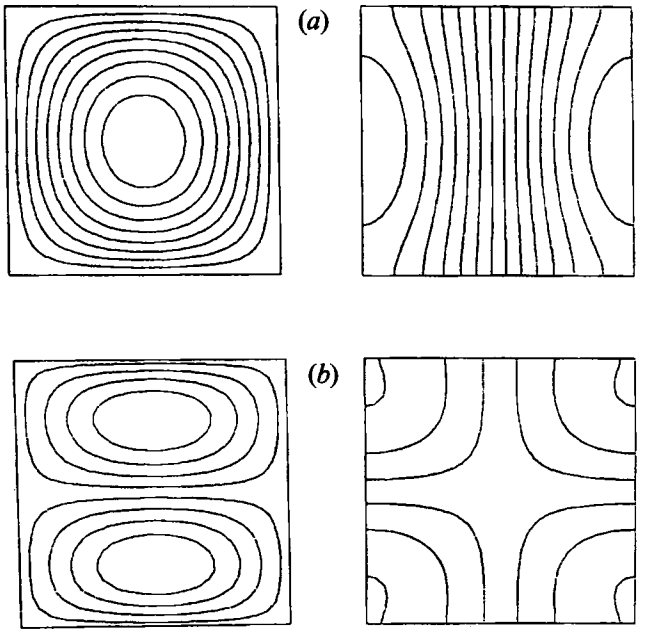

FIGURE 2. Eigensolutions for the perturbation streamfunction and temperature for (*a*) the $(1, \lambda_{1,1})$ mode, (*b*) the $(1, \mu_{1,1})$ mode.

which satisfy (15)–(17) provided that $\lambda_{m,n}$ and $\mu_{m,n}$ satisfy, respectively,

$$(\lambda^2 + 2m^2\pi^2/A^2)^{1/2} \tanh \tfrac{1}{2}(\lambda^2 + 2m^2\pi^2/A^2)^{1/2} = \lambda \tan \tfrac{1}{2}\lambda, \tag{20}$$

$$(\mu^2 + 2m^2\pi^2/A^2)^{1/2} \coth \tfrac{1}{2}(\mu^2 + 2m^2\pi^2/A^2)^{1/2} = -\mu \cot \tfrac{1}{2}\mu. \tag{21}$$

Eigenmodes will therefore arise when the Rayleigh number satisfies

$$Ra_{m,n} = \frac{\pi^2}{(m/A)^2}\left(\frac{\lambda_{m,n}^2}{\pi^2} + (m/A)^2\right)^2, \quad \frac{\pi^2}{(m/A)^2}\left(\frac{\mu_{m,n}^2}{\pi^2} + (m/A)^2\right)^2, \tag{22}$$

which is similar to Sutton's (1970) result for the onset of convection in a porous medium between horizontal isothermal boundaries, except that the wavenumber in y is now, in general, non-integral and dependent on the wavenumber in x and the aspect ratio. For the present flow, the neutral stability curves possess geometrical similarity, arising as a consequence of the slip boundary conditions, as in the isothermal case; that is,

$$Ra_{m,n}(mA) = Ra_{1,n}(A), \tag{23}$$

so that a unicellular flow in a cavity of aspect ratio A will be identical to one of the cells in the m-cellular flow in cavity of aspect ratio mA, provided that the Rayleigh numbers are the same.

In order to determine the critical Rayleigh number (Ra_{cr}) for onset, we consider the solutions to (20) and (21). For all values of m and A, equation (20) has a unique solution, $\lambda_{m,n}$, on each of the intervals $((2n-2)\pi, (2n-1)\pi)$, for $n = 1, 2, \ldots$; similarly equation (21) has a unique solution, $\mu_{m,n}$, on each of the intervals $((2n-1)\pi, 2n\pi)$, from which it is clear that $\lambda_{m,n} < \mu_{m,n}$ for all values of m, n and A, so that by equation (22) it will be one of the $(m, \lambda_{m,n})$, rather than $(m, \mu_{m,n})$, modes which destabilizes the pure conductive state. Physically, this implies that a flow with m cells in the horizontal direction and $2n-1$ cells in the vertical, corresponding to the $(m, \lambda_{m,n})$ mode, destabilizes the conductive state ahead of a flow with m horizontal cells but $2n$ vertical cells, corresponding to the $(m, \mu_{m,n})$ mode. In figures 2(*a*) and 2(*b*) we show the

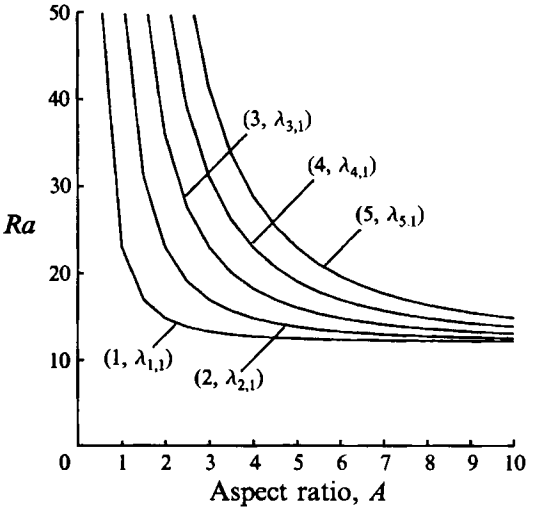

FIGURE 3. Critical Rayleigh number for the onset of convection for the leading eigenmodes as a function of aspect ratio.

eigenfunctions for the streamfunction (on the left) and the temperature (on the right), respectively corresponding to the $(1,\lambda_{1,1})$-mode, for which $\lambda_{1,1} \approx 2.276$ and $Ra_{cr} \approx 22.946$, and the $(1,\mu_{1,1})$-mode, for which $\mu_{1,1} \approx 5.002$ and $Ra_{cr} \approx 123.309$, for the case $A = 1$. Furthermore, by the properties of the functions in (20), it is evident that for all n and A, $\lambda_{m,n} < \lambda_{m+1,n}$, in addition to which, since $\lambda_{m,n} < \lambda_{m,n+1}$, we note that criticality will be determined by the modes involving $n = 1$.

We plot in figure 3 the critical Rayleigh number against the aspect ratio for several of the leading modes, from which it is clear that $(1,\lambda_{1,1})$ remains the destabilizing mode for all values of A, ahead of the other $(m,\lambda_{m,1})$ modes ($m \geqslant 2$), and that the ordering of these modes, in the sense that $Ra_{m,1} < Ra_{m+1,1}$, is preserved as A increases; in particular, we also note that as $A \to \infty$, the limiting value of $Ra_{cr} = 12$ (Nield 1968) is approached monotonically. The results are therefore in contrast to the case for isothermal boundary conditions, where not only does the destabilizing mode change as the aspect ratio increases, but the behaviour of the critical Rayleigh number is non-monotonic with increasing aspect ratio (Riley & Winters 1989). For constant-flux boundary conditions, therefore, unicellular flow remains a stable convective mode for all values of A, whilst for the isothermal case unicellular flow is ruled out on the grounds of instability for $A > \sqrt{2}$; this goes some way towards explaining why unicellular, rather than multicellular, flows were observed in the computations of this paper.

For the moment, as a precursor to those computations, we consider the flow for infinite aspect ratio for Ra in excess of 12.

3.2. *Solution for fully developed two-dimensional counterflow*

As given by Bejan (1983) for a vertical cavity, and later adopted by Vasseur *et al.* (1987) and Sen *et al.* (1987) for inclined cases, one may assume the existence of a two-dimensional fully developed counterflow, which may be a good approximation for the mid-region of the horizontally extended space provided that unicellular convection is stable. For the temperature, the following form may be assumed:

$$T(x,y) = Sx + \theta(y), \tag{24}$$

where S is a constant representing the temperature gradient in the horizontal direction and θ is the variation in the vertical direction. Since the flow is fully developed, the velocity in the x-direction is a function of y only, and there is no velocity in the y-direction, so that

$$\boldsymbol{q} = (U(y), 0, 0). \tag{25}$$

Substituting the above expressions for the temperature and velocity into the governing equations (2) and (3), cross-differentiating to eliminate the pressure, integrating and using boundary condition (7) only, it is straightforward to derive the solutions for U and θ as

$$U(y) = \tfrac{1}{2}Ra\,S(1-2y), \tag{26}$$

$$\theta(y) = \tfrac{1}{2}Ra\,S^2(\tfrac{1}{2}y^2 - \tfrac{1}{3}y^3 - \tfrac{1}{12}) - y + \tfrac{1}{12}. \tag{27}$$

The constant S appearing in the above solutions can be obtained by imposing a constraint that the enthalpy flux at a vertical cross-section at any horizontal position must be zero (Bejan 1983), that is

$$\int_0^1 \left(uT - \frac{\partial T}{\partial x}\right) \mathrm{d}y = 0.$$

Together with equations (26) and (27), this yields an expression for S in terms of Ra:

$$S = \pm\left[\frac{10}{Ra}\left(1 - \frac{12}{Ra}\right)\right]^{1/2}. \tag{28}$$

In the following, we take the positive sign for S, so that the flow is anticlockwise in orientation; the negative sign leads to clockwise flow, with otherwise identical results. Equations (26) and (27) and the expressions for S constitute the flow and temperature solutions when a fully developed flow in a horizontal cavity is assumed; the solution is the same as that obtained by Sen *et al.* (1987) as a special case for more general fully developed counterflow with arbitrary inclination to the direction of gravitational acceleration. Our primary concern, however, is whether or not this unicellular solution can stably exist at an arbitrarily high Rayleigh number and, if not, what kind of transition from the unicellular convecting flow may be expected at criticality. It is worth mentioning that the flow and temperature solutions obtained from equations (26)–(28) are qualitatively similar to those with horizontal and vertical temperature gradients (Weber 1974; Nield 1991). However, the present problem involves only a single parameter, the Rayleigh number based on flux strength, whereas that studied by Weber (1974) and Nield (1991) has two independent parameters: the Rayleigh numbers based on the vertical and horizontal temperature gradients.

A physically important quantity in heat transfer processes is the Nusselt number Nu, which is defined by the ratio of the actual heat flux to the transferred heat if conduction were the sole mechanism driving heat flow. By this definition, Nu is written as

$$Nu = \frac{Q''}{k_e(T_l^* - T_u^*)/H} = \frac{1}{T_l - T_u}, \tag{29}$$

where the subscripts l and u indicate the lower and upper boundaries respectively. Since the upper and lower boundary temperature may in general vary along the x-axis, it should be remembered that the aforementioned analytical solution will cease to be valid in the extreme end regions.

3.3. *Linear stability analysis*

Letting

$$\left.\begin{aligned} \boldsymbol{q} &= U(y)\,\boldsymbol{i}+\hat{\boldsymbol{q}}(x,y,z,t),\\ T &= \theta(y)+Sx+\hat{\theta}(x,y,z,t),\\ p &= P(x,t)+\hat{p}(x,y,z,t), \end{aligned}\right\} \tag{30}$$

where $\boldsymbol{i}$ is the unit vector in the x-direction, and once again assuming that the perturbation quantities are small, we substitute into equations (1)–(3) and linearize to obtain

$$\nabla\cdot\hat{\boldsymbol{q}} = 0, \tag{31}$$

$$\nabla\hat{p}+\hat{\boldsymbol{q}}-Ra\,\hat{\theta}\boldsymbol{j} = 0, \tag{32}$$

$$\partial\hat{\theta}/\partial t+U\partial\hat{\theta}/\partial x+\hat{v}\theta'+S\hat{u}-\nabla^2\hat{\theta} = 0, \tag{33}$$

where the prime denotes differentiation with respect to y, and the components of the perturbation velocity $\hat{\boldsymbol{q}}$ are $(\hat{u},\hat{v},\hat{w})$. Now we make a normal mode expansion by letting

$$(\hat{u},\hat{v},\hat{w},\hat{\theta},\hat{p}) = (\tilde{u}(y),\tilde{v}(y),\tilde{w}(y)\,\tilde{\theta}(y),\tilde{p}(y))\,\mathrm{e}^{\sigma t+\mathrm{i}(kx+lz)},$$

and substitute into equations (31)–(33). Eliminating $\tilde{u}(y)$, $\tilde{w}(y)$ and $\tilde{p}(y)$ and writing

$$\alpha^2 = k^2+l^2,$$

we obtain the ordinary differential equations

$$\tilde{v}''-\alpha^2\tilde{v}+Ra\,\alpha^2\tilde{\theta} = 0, \tag{34}$$

$$\tilde{\theta}''-(\alpha^2+\mathrm{i}kU+\sigma)\,\tilde{\theta}-(\mathrm{i}Sk/\alpha^2)\,\tilde{v}'-\tilde{v}\theta' = 0. \tag{35}$$

Equations (34) and (35) are subject to the boundary conditions

$$\tilde{v} = 0 \quad \text{at} \quad y = 0 \quad \text{and} \quad 1, \tag{36}$$

$$\tilde{\theta}' = 0 \quad \text{at} \quad y = 0 \quad \text{and} \quad 1, \tag{37}$$

so that equations (34)–(37) constitute an eigenvalue problem for Ra.

In general, an analytical solution to the above equations is not possible, and so numerical means are necessary. At least two methods are possible: either a direct solution of the equations using Runge–Kutta and shooting techniques or using a Galerkin expansion, which is the method we indicate here. Writing the expansions for $\tilde{v}$ and $\tilde{\theta}$ as

$$\tilde{v}(y) = \sum_{n=1}^{N} A_n \sin n\pi y, \tag{38}$$

$$\tilde{\theta}(y) = \sum_{n=0}^{N-1} B_n \cos n\pi y, \tag{39}$$

respectively, where the forms for equations (38) and (39) have been chosen in order to satisfy (36) and (37), and N is the truncation level, we then substitute into (34) and (35) and re-expand sine terms and powers of y using a cosine series. Equation (34) then reduces to the N equations

$$B_{m-1} = \sum_{n=1}^{N} T_{mn}\,A_n, \quad m = 1,\ldots,N, \tag{40}$$

where

$$T_{mn} = \begin{cases} \dfrac{2}{\pi\,Ra\,k^2}\,\dfrac{n(k^2+n^2\pi^2)(1+(-1)^{n+m})}{n^2-(m-1)^2} & \text{if} \quad m \geqslant 2\\[2ex] \dfrac{1}{\pi\,Ra\,k^2}\,\dfrac{(k^2+n^2\pi^2)(1-(-1)^n)}{n} & \text{if} \quad m = 1. \end{cases}$$

Similarly (35) becomes

$$\sum_{n=1}^{N} \mu_{mn} B_{n-1} - \sigma B_{m-1} = \sum_{n=1}^{N} \lambda_{mn} A_n, \quad m = 1, \ldots, N, \tag{41}$$

where

$$\lambda_{mn} = \begin{cases} Ra\, S^2 (P_{mn} - Q_{mn}) - 2R_{mn} + \dfrac{iS(m-1)}{k} \delta_{nm-1} & \text{if} \quad m \geqslant 2 \\ \left(\dfrac{Ra\, S^2}{n^2 \pi^2} - 1 \right) \dfrac{1-(-1)^n}{n\pi} & \text{if} \quad m = 1, \end{cases}$$

$$\mu_{mn} = \begin{cases} 2ikRa\, S_{mn} - (k^2 + (m-1)^2 \pi^2 + \frac{1}{2} ik\, Ra\, S & \text{if} \quad m \geqslant 2, \\ -k^2 - \dfrac{ik\, Ra\, S}{\pi^2} (1 - (-1)^n) & \text{if} \quad m = 1, \end{cases}$$

and

$$P_{mn} = \begin{cases} \dfrac{-1}{2(n+m-1)\pi} & \text{if} \quad n = m-1 \\ \dfrac{(-1)^{n+m} n}{(n^2 - (m-1)^2)\pi} & \text{otherwise,} \end{cases}$$

$$Q_{mn} = \begin{cases} \dfrac{-1}{2(n+m-1)\pi} & \text{if} \quad n = m-1 \\ \dfrac{(-1)^{n+m} n}{\pi(n^2 - (m-1)^2)} - \dfrac{2n(n^2 + 3(m-1)^2)((-1)^{n+m} + 1)}{(n^2 - (m-1)^2)^3} & \text{otherwise,} \end{cases}$$

$$R_{mn} = \begin{cases} 0 & \text{if} \quad n = m-1 \\ \dfrac{(1 + (-1)^{n+m}) n}{\pi(n^2 - (m-1)^2)} & \text{otherwise,} \end{cases}$$

$$S_{mn} = \begin{cases} \frac{1}{4} & \text{if} \quad n = m-1 \\ -\dfrac{((-1)^{n+m} + 1)((m-1)^2 + n^2)}{\pi^2 ((m-1)^2 - n^2)^2} & \text{otherwise,} \end{cases}$$

and δ_{mn} denotes the Kronecker delta given by

$$\delta_{mn} = \begin{cases} 1 & \text{if} \quad n = m \\ 0 & \text{otherwise.} \end{cases}$$

Thence on inverting the matrix T_{mn} in equation (40) we obtain

$$A_m = \sum_{n=1}^{N} T_{mn}^{-1} B_{n-1}, \quad m = 1, \ldots, N, \tag{42}$$

which, on substituting into (41) gives

$$[\boldsymbol{U} - \sigma \boldsymbol{I}] \boldsymbol{b} = 0, \tag{43}$$

where the elements, U_{mn}, of the matrix $\boldsymbol{U}$ are given by

$$U_{mn} = \mu_{mn} - \sum_{j=1}^{N} \lambda_{mj} T_{jn}^{-1},$$

$\boldsymbol{I}$ is the identity matrix and $\boldsymbol{b} = (B_0, B_1, \ldots, B_{N-1})^T$. Equation (43) was solved using the

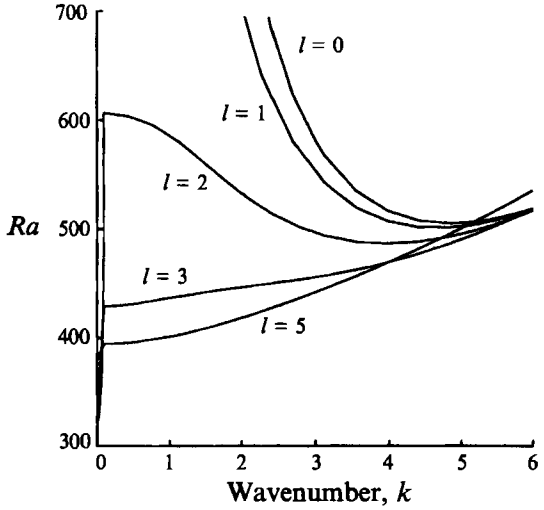

FIGURE 4. Critical Rayleigh number for the destabilization of fully developed flow against the x-wavenumber (k) for different values of the z-wavenumber (l).

N	k_{cr}	Ra_{cr}	f_{cr}
30	4.834	502.68	22.09
60	4.828	505.21	22.11
90	4.826	505.69	22.11
∞	4.825	506.07	22.11

TABLE 1. Effect of truncation level, N, on determining critical instability for Galerkin method

NAG routine F02AJF for various values of Ra, k and l in order to determine the exponential growth rate, σ. In addition, the truncation level, N, was varied and the results checked against those obtained by solving equations (34)–(37) directly using Runge–Kutta and shooting methods. In order to determine the critical Rayleigh number for the onset of instability, the values of k and l were fixed and the value of Ra for which $\mathrm{Re}(\sigma) = 0$ was determined using a bisection method; in general, of course, for a particular value of Ra, there will be N solutions for σ, but it is evident that the relevant one here is that with maximal real part. This procedure was carried out for a suite of values of k and l, and the combination of k and l which gave the lowest value for Ra_{cr} was deemed to provide the critical wavenumbers, k_{cr} and l_{cr}, in the x- and z-directions, respectively, with Ra_{cr} thence obviously the critical Rayleigh number.

In the first instance, two-dimensional disturbances, corresponding to $l = 0$, were considered. It was found that the base velocity and temperature profiles are stable for values of Ra less than 506, at which point an instability via a Hopf bifurcation, as evidenced by a critical eigenvalue with zero real part, i.e. $\mathrm{Re}(\sigma) = 0$, and non-zero imaginary part ($\mathrm{Im}(\sigma)$), sets in; the quantity $\mathrm{Im}(\sigma)/2\pi$ is in fact the critical oscillation frequency, f_{cr}. In table 1 we show the results obtained for $N = 30$, 60 and 90, and compare these with those obtained by solving the differential equations; evidently, as N is increased, the results coincide with those of the Runge–Kutta method, as one would wish. Subsequently, three-dimensional disturbances were considered, with the value of l being gradually increased from zero; figure 4 illustrates the trends that were observed, and in particular how the two-dimensional Hopf bifurcation (on the line

$l = 0$) fits into the three-dimensional analysis. For $l > 0$, the stability analysis indicates that the counterflow will be destabilized not by a Hopf bifurcation, but by an exchange of stability for which $k = 0$. In particular, as l decreases, so does Ra_{cr} on $k = 0$ (the curve for which $l = 1$ would also show a steep jump near $k = 0$ in the manner of the curves $l = 2, 3, 5$ had we computed it for smaller values of k). For values of k within the region of steep ascent, exchange of stability occurs; for greater values of k, there is a Hopf bifurcation for which $|\mathrm{Im}(\sigma)|$ increases with k. As l is increased from zero, Ra_{cr} and k_{cr} for the Hopf bifurcation are found to decrease until $l \approx 2.725$, corresponding to $Ra_{cr} \approx 464.32$ with $k_{cr} \approx 2.12$; thereafter, there is no local minimum for Ra, so that, for example, Ra for the $l = 3$ and $l = 5$ curves decreases monotonically with k to attain its minimum value at $k = 0$. From figure 4, since it is clear that criticality occurs at $k = 0$, we are led to consider disturbances in the z-direction only.

The governing equations now simplify to

$$\tilde{v}'' - l^2\tilde{v} + Ra\, l^2\tilde{\theta} = 0, \tag{44}$$

$$\tilde{\theta}'' - (l^2 + \sigma)\tilde{\theta} - \tilde{v}\theta' = 0, \tag{45}$$

subject to the boundary conditions (36) and (37). The numerical solution used for determining the values of Ra at $k = 0$ indicates that the value of Ra_{cr} increases monotonically with $l(> 0)$, so that the critical wavenumber is therefore $l = 0$. In this case, we are actually able to determine the critical Rayleigh number analytically, as follows. Writing $\tilde{v}$, $\tilde{\theta}$, Ra and σ as expansions in l^2, so that

$$\tilde{v} = \tilde{v}_0 + l^2\tilde{v}_2 + l^4\tilde{v}_4 + \ldots,$$

$$\tilde{\theta} = \tilde{\theta}_0 + l^2\tilde{\theta}_2 + l^4\tilde{\theta}_4 + \ldots,$$

$$Ra = Ra_0 + l^2 Ra_2 + l^4 Ra_4 + \ldots,$$

$$\sigma = \sigma_0 + l^2\sigma_2 + l^4\sigma_4 + \ldots,$$

we substitute into equations (44) and (45) to obtain, at $O(l^0)$,

$$\tilde{v}_0 = 0, \quad \tilde{\theta}_0 = \text{constant}$$

(which may be taken to be 1 without loss of generality) and $\sigma_0 = 0$; evidently, $l = 0$ is a critical value, although higher orders of l need to be considered in order to determine the nature of the criticality and the corresponding Rayleigh number.

At $O(l^2)$, the governing equations are

$$\tilde{v}_2'' - \tilde{v}_0 + Ra_0\tilde{\theta}_0 = 0, \tag{46}$$

$$\tilde{\theta}_2'' - (1 + \sigma_2)\tilde{\theta}_0 - \sigma_0\tilde{\theta}_2 - \tilde{v}_2\theta_0' - \tilde{v}_0\theta_2' = 0, \tag{47}$$

with $\tilde{\theta}_2$ and $\tilde{v}_2$ subject to the boundary conditions (36) and (37), and where $\theta'(y)$ has been expanded in l^2, according to

$$\theta' = \theta_0' + l^2\theta_2' + \ldots,$$

with $$\theta_0'(y) = 5\left(1 - \frac{12}{Ra_0}\right)(y - y^2) - 1, \quad \theta_2'(y) = \frac{60Ra_2}{Ra_0^2}(y - y^2).$$

Thence, $$\tilde{v}_2(y) = \tfrac{1}{2}Ra_0(y - y^2),$$

which, on inserting into (47) and integrating over [0, 1] gives $\sigma_2 = 0$; it is therefore necessary to go to $O(l^4)$, although we need first to observe that

$$\tilde{\theta}_2(y) = \frac{y^2}{2} + \frac{Ra_0}{2}\left(5\left(1 - \frac{12}{Ra_0}\right)\left(\frac{y^4}{12} - \frac{y^5}{10} + \frac{y^6}{30}\right) - \frac{y^3}{6} + \frac{y^4}{12}\right) + C,$$

where C is a constant whose value ultimately will not need to be determined.

At $O(l^4)$, the governing equations are

$$\tilde{v}_4'' - \tilde{v}_2 + Ra_0\tilde{\theta}_2 + Ra_2\tilde{\theta}_0 = 0, \tag{48}$$

$$\tilde{\theta}_4'' - \sigma_4\tilde{\theta}_0 - \tilde{\theta}_2 - \tilde{v}_0\theta_4' - \tilde{v}_2\theta_2' - \tilde{v}_4\theta_0' = 0, \tag{49}$$

whereupon we obtain, on integrating the first of these twice and applying the boundary conditions,

$$\tilde{v}_4(y) = \frac{Ra_0}{12}(y^3 - y^4) - \frac{Ra_2}{2}y^2 + Ey$$

$$- Ra_0\left(\frac{C}{2}y^2 + \frac{Ra_0}{2}\left(5\left(1 - \frac{12}{Ra_0}\right)\left(\frac{y^6}{360} - \frac{y^7}{420} + \frac{y^8}{1680}\right) - \frac{y^5}{120} + \frac{y^6}{120}\right)\right),$$

where

$$E = \frac{Ra_2}{2} + Ra_0\left(\frac{C}{2} + \frac{5}{168} - \frac{Ra_0}{3360}\right).$$

Integrating (49) over [0, 1] and applying the boundary conditions for $\tilde{\theta}_4'$, we find that integrals involving Ra_2, C and D cancel, leaving just the relation

$$\sigma_4 = \frac{1}{36}\left(\frac{Ra_0^2}{18480} - \frac{Ra_0}{165} - \frac{37}{11}\right); \tag{50}$$

for criticality, we set $\sigma_4 = 0$, and solve to obtain the roots for Ra_0 as

$$Ra_0 = 56 \pm 4\sqrt{4081},$$

the positive one of which, approximately $Ra_{cr} \approx 311.53$, is the physically relevant one. Furthermore, if we set Ra_0 slightly greater than this value in equation (50), we find that σ_4 is real and positive, indicating an exchange of stability. Since this critical Rayleigh number is much lower than any of those for the Hopf bifurcations obtained earlier when $k \neq 0$, we conclude that the counterflow will in fact be destabilized by longitudinal, rather than transverse, disturbances; this would appear to be in line with the results of Nield (1991) for a Hadley-type cell in which the temperature, rather than the temperature gradient, is prescribed at $y = 0, 1$.

The above analysis for a region of infinite extent in the z-direction may be added to by considering the case where the porous medium is confined to lie between the planes $z = 0$ and $z = z_0$, across which there is no heat or fluid flow; in this case the normal mode expansion is written as

$$(\hat{u}, \hat{v}, \hat{\theta}, \hat{p}) = (\tilde{u}(y), \tilde{v}(y), \tilde{\theta}(y), \tilde{p}(y))\, e^{\sigma t + \mathrm{i}kx} \cos(m\pi z/z_0),$$

$$\hat{w} = \tilde{w}(y)\, e^{\sigma t + \mathrm{i}kx} \sin(m\pi z/z_0),$$

and the governing equations are still (44) and (45), except with l now replaced by $m\pi/z_0$ and m integral. To find Ra_{cr}, it is clear that we should take $m = 1$, and so we plot the

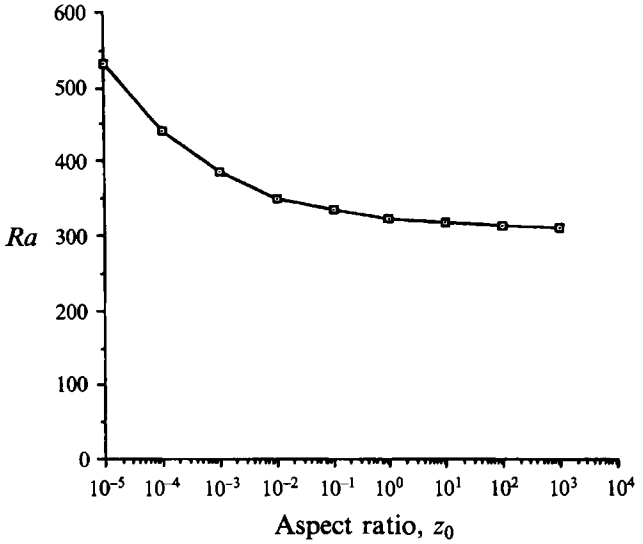

FIGURE 5. Critical Rayleigh number against aspect ratio in the z-direction (z_0).

dependence of Ra_{cr} on z_0 in figure 5; as one might expect, Ra_{cr} increases as z_0 decreases, which gives rise to the possibility that for sufficiently small z_0 the two-dimensional Hopf bifurcation discussed earlier may set in in advance of the exchange of stability. From figure 5, $Ra \approx 506$ corresponds to $z_0 \approx 1.5 \times 10^{-5}$: a bound on the aspect ratio, z_0, that is possibly difficult to realize experimentally.

Furnished with a linear stability analysis to indicate the nature of the flow as Ra is increased, we proceed to a numerical solution of the full two-dimensional equations for the case of finite aspect ratio, for which the results for the Hopf bifurcation at $Ra \approx 506$ will be the most relevant.

4. Numerical analysis

4.1. *Numerical procedure*

Introducing a streamfunction, ψ, and rewriting the governing equations (1)–(3) in the form

$$\nabla^2\psi = -Ra\,\partial T/\partial x, \tag{51}$$

$$\frac{\partial T}{\partial t}+\frac{\partial \psi}{\partial y}\frac{\partial T}{\partial x}-\frac{\partial \psi}{\partial x}\frac{\partial T}{\partial y}=\nabla^2 T, \tag{52}$$

we discretize (51) and (52) using Patankar's (1980) control-volume method. The aspect ratio of the rectangular computational domain was taken to be $A = 2$, 4 8 and 10; as an example of the meshes used for the computation, the domain was covered by a grid of 19×101 points for $A = 4$ and 19×201 for $A = 8$. The code was validated by generating a unicellular counterflow and comparing the results with those of the analytical solutions derived in the previous section. It was found that the velocity was rather insensitive to grid refinement. On the other hand, the temperature field was found to be extremely sensitive to computational resolution: for example, the relative difference between the numerical velocity profile in y, when a relatively coarse 15×51 grid was used, and the analytical distribution at $x = 0$ for $Ra = 400$ was found to be within 5%, whilst the numerically predicted Nusselt number was around 10% lower

	Analytical		Numerical results at $x = 0$					
			Nu			ψ_{max}		
Ra	Nu	ψ_{max}	15×51	19×101	21×101	15×51	19×101	21×101
100	3.750	3.708	3.379	3.544	4.544	3.824	3.756	3.739
200	4.615	5.420	4.089	4.367	4.366	5.572	5.467	5.447
400	5.217	7.786	4.578	4.946	4.957	7.979	7.828	7.796
500	5.357	8.732	4.695	5.086	5.101	8.934	8.764	8.729
600	5.455	9.585	4.778	5.188	5.207	9.787	9.600	9.562
700	5.526	10.368	4.843	5.266	5.288	10.564	10.360	10.320

TABLE 2. Effect of grid size on numerical accuracy ($A = 4$)

than that given by the analytical solution. Subsequently, it was found that adequate agreement for Nu could only be obtained if the grid consisted of at least 19 points in the y-direction and at least 101 in the x-direction. Numerical accuracy was also found to be sensitive not only to grid resolution in the vertical direction, particularly near the top and bottom boundaries, but also in the horizontal; for instance, a grid containing 19 points in the y-coordinate and 51 in the x-coordinate for aspect ratio 4 failed to improve upon, relative to the 15×51 mesh, the value of the Nusselt number at $x = 0$, and it required at least 101 grid points in the x-direction as well in order to reduce the relative difference to the order of 5%. The overall effect of grid resolution on numerical accuracy is collated in table 2. We note that in order to avoid any bias towards preferred convection patterns, we used uniform grid spacing in the x-direction; for the y-coordinate, on the other hand, non-uniform spacing was allowed. Near the horizontal boundaries, typically the grid spacing was 0.006 in y and 0.04 in x.

The Poisson equation for the streamfunction was solved using a vectorized version of the SOR method, which essentially relies on a sweeping process in a diagonal direction over the grid network which permits the use of renewed values line by line at each iteration. The energy equation was integrated explicitly in time; a typical integration time step for computations employing 19 grid points in the y-coordinate was $\Delta t = 2.5 \times 10^{-5}$, whilst for 21 grid points the time step was reduced to $\Delta t = 1 \times 10^{-5}$. For a few cases, the time step was halved in order to verify that the solution did not depend on Δt. The convergence of SOR was determined by the following criterion:

$$\frac{\sum_{i}^{K}\sum_{j}^{L}|\psi_{ij}^{n+1}-\psi_{ij}^{n}|}{\sum_{i}^{K}\sum_{j}^{L}|\psi_{ij}^{n+1}|} \equiv Res \leqslant \epsilon, \tag{53}$$

where ϵ was taken as 10^{-6}, K and L are the number of mesh points in the x- and y-directions respectively, and n is the iteration number. A similar criterion was used for T_{ij} to judge whether steady state had been reached. All computations were carried out in double precision using a Titan engineering work station, equipped with a vector processor.

4.2. *Numerical results for unicellular steady convection*

From equation (28), it is clear that the analytical solution for fully developed flow is possible only when Ra is greater than 12. This critical value agrees with Nield's (1968) result concerning the criticality for the onset of convection from a conducting steady

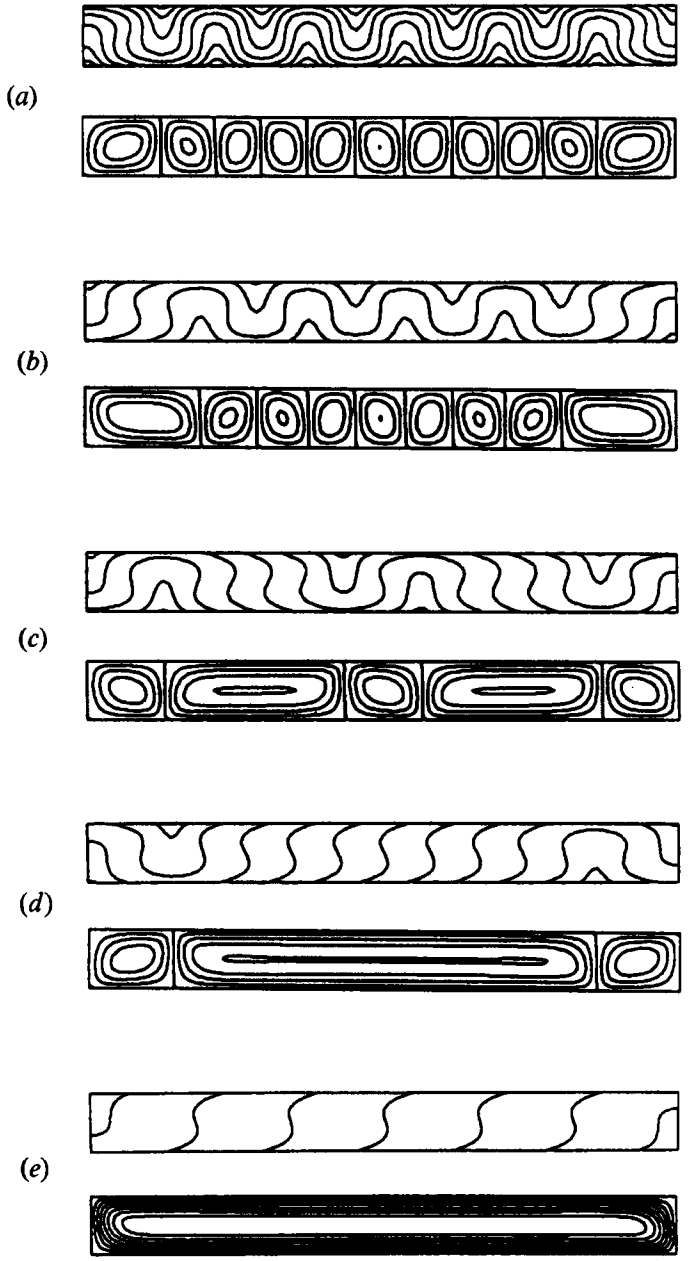

FIGURE 6. Time-dependent velocity and temperature-field evolution towards unicellular convection ($Ra = 100, A = 10$): (*a*) $t = 2.5$ ($\Delta\theta = 0.1, \Delta\psi = 1$); (*b*) $t = 7.5$ ($\Delta\theta = 0.1, \Delta\psi = 1$); (*c*) $t = 57.5$ ($\Delta\theta = 0.2, \Delta\psi = 1$); (*d*) $t = 107.5$ ($\Delta\theta = 0.25, \Delta\psi = 1$); (*e*) $t = 157.5$ ($\Delta\theta = 0.5, \Delta\psi = 0.5$).

state. For finite aspect ratio, our numerical results show that the conductive state is stable when the Rayleigh number is smaller than 12, so that perturbations imposed on the conducting solution always decay as the time integration progresses. Computations carried out for Ra in excess of 12 were found to agree with (22); for instance, for $Ra = 20$, $A = 10$, the numerical solution evolves towards a convective steady state, as one would expect for $Ra > Ra_{cr}$ (in this case, $Ra_{cr} \approx 12.11$). Figure 6 is typical of the transient development of the velocity and temperature fields from zero initial

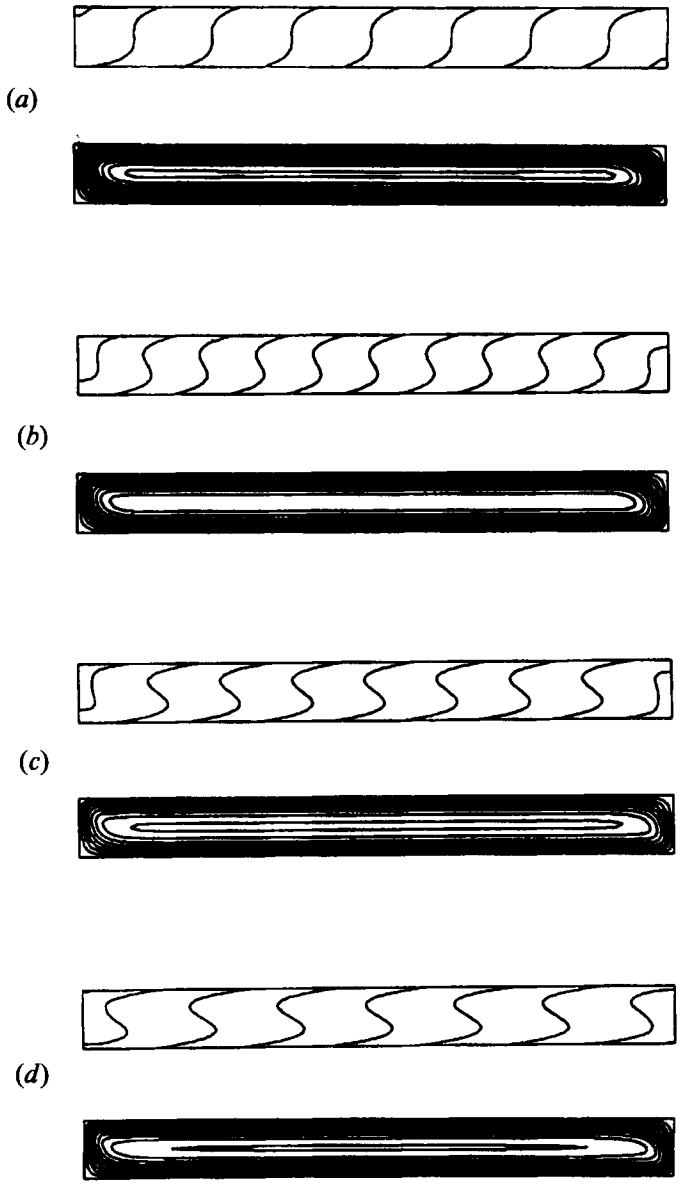

FIGURE 7. Variation of single-cell solution with Rayleigh number: (*a*) $Ra = 65$ ($\Delta\theta = 0.5, \Delta\psi = 0.25$); (*b*) $Ra = 150$ ($\Delta\theta = 0.5, \Delta\psi = 0.5$); (*c*) $Ra = 400$ ($\Delta\theta = 0.2, \Delta\psi = 2$); (*d*) $Ra = 600$ ($\Delta\theta = 0.2$, $\Delta\psi = 2$).

conditions; we mention in passing that for this and subsequent computations, no artificial disturbance was introduced, so that convection essentially evolved from numerical noise. When the value of the Rayleigh number is increased, there are initially a number of convecting cells whose horizontal dimension has roughly the same order of magnitude as the height of the cavity. These convecting cells gradually merge together to form horizontally elongated cells, and eventually a single cell. The time taken for the attainment of a steady state is found to be independent of Ra if the initial conditions are taken to be zero everywhere, but dependent instead on the geometrical aspect ratio; for instance, if $A = 8$, the dimensionless time required to reach a steady

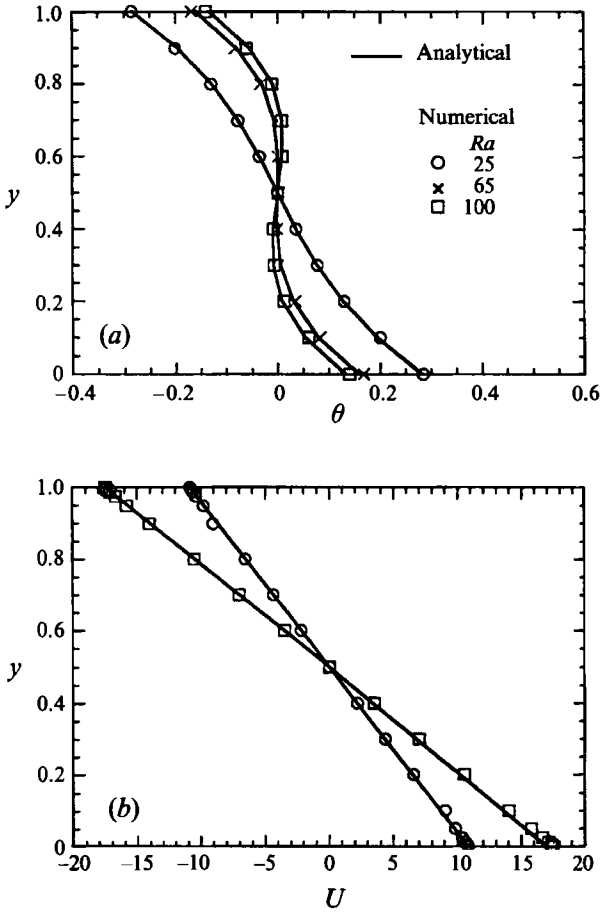

FIGURE 8. Comparison of analytical solutions for the fully developed regime with numerical results at $x = 0$ for small Rayleigh number: (*a*) θ, (*b*) U.

state is 130, whereas if $A = 4$, this value is approximately halved. This is the same order of magnitude in time as it takes for heat to diffuse horizontally over the entire space.

In figure 6, it should be noted that during the transient process the flow evolves in a centro-symmetric manner. It is also seen that there exists a linear horizontal temperature gradient over the cavity, on which local temperature variations due to individual convecting cells are superposed. The Nusselt number during the transient state is on average lower than at steady state; this is observed by dint of the fact that the isotherms are less closely spaced at steady state. Furthermore, the convecting velocity at $x = 0$ becomes greatest at steady state. Unicellular convection at steady state (figure 6*e*) exhibits a linear horizontal temperature gradient over the space superposed by a nonlinear vertical temperature variation that is independent of the x-coordinate, and is such that the greatest part consists of a fully developed counterflow, except for the narrow end regions where the velocity field is turned around. All the properties of the numerically computed temperature and flow fields at steady state support the assumptions made earlier for deriving the analytical solution. Figure 7 indicates a series of unicellular convection patterns at steady state for four different values of *Ra*. No qualitative differences can be observed among the four as regards the flow structure, with both temperature and velocity fields keeping their basic

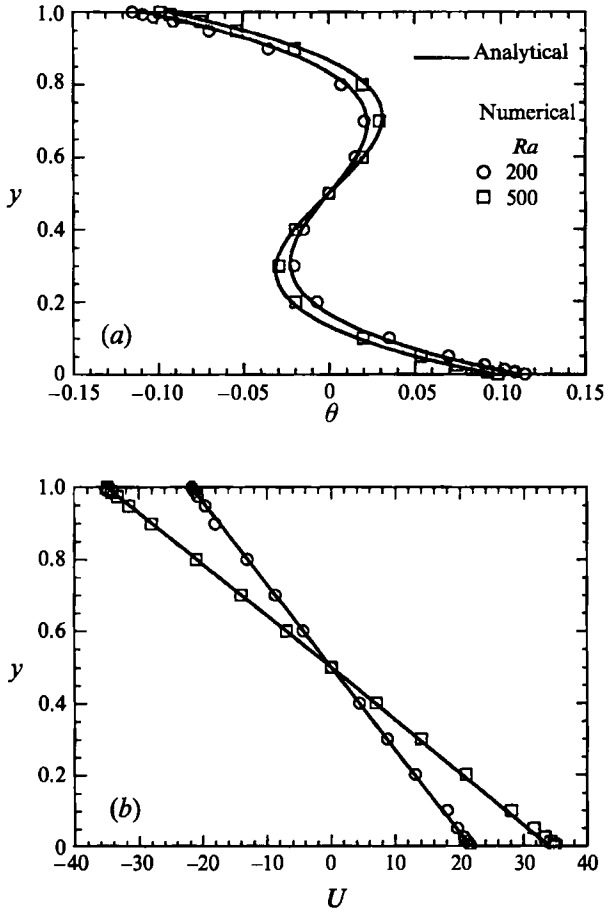

FIGURE 9. Comparison of analytical solutions for the fully developed regime with numerical results at $x = 0$ for large Rayleigh number: (*a*) θ, (*b*) U.

structure regardless of Ra; quantitatively, fluid velocity increases appreciably with Ra, although the change in temperature is not so marked. However, both the difference between the top and bottom boundary temperatures and the horizontal temperature gradient decrease with increasing Ra, and the vertical temperature variation becomes increasingly nonlinear with Ra.

4.3. *Comparison with the analytical solution*

In this section, we compare extensively the numerical solutions with the analytical solutions developed in §3.1. Figure 8 shows the numerical and analytical results for relatively low Rayleigh numbers. Regarding the vertical temperature variation $\theta(y)$, it is easy to show from equations (27) and (28) that $\theta(y)$ has an inflection point at $y = 0.5$ when the Rayleigh number is greater than 60. This is seen in figure 8(*a*); at $Ra = 25$, the temperature decreases monotonically with y, whereas for $Ra = 65$ there is a region near $y = 0.5$ where the temperature undergoes inflection. This behaviour is reproduced exactly by the full numerical results. The analytical results for $\theta(y)$ for low Rayleigh numbers ($Ra = 25$, 65 and 100) agree well with the full numerical solutions. According to equation (26), the velocity $U(y)$ is linear, and so is the corresponding numerical solution. In figure 9, we show the comparisons for higher Rayleigh numbers, $Ra = 200$

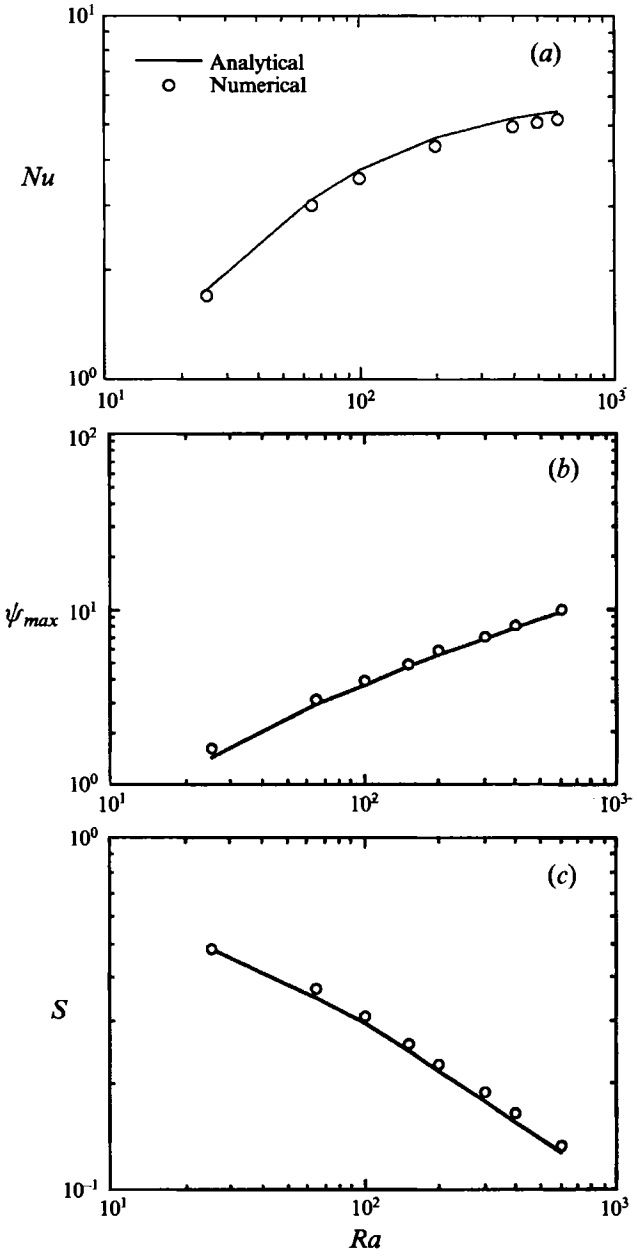

FIGURE 10. Analytical solution for (*a*) Nusselt number, (*b*) ψ_{max}, and (*c*) S, as functions of the Rayleigh number, compared with numerical results at $x = 0$.

and 500; the inflection point for $\theta(y)$ at $y = 0.5$ becomes more evident (figure 9*a*). The linear velocity profiles, in general, display good agreement with the numerical ones.

The Nusselt number variation with Rayleigh number is shown in figure 10(*a*); in general, the numerical solutions tend to underestimate the value for Nu at $x = 0$ that is predicted analytically. The differences between the two, however, are about 5%, and do not vary much with Ra. These differences may in part be due to the finite horizontal extent of the domain used for numerical computation. In figure 10(*b*) the maximum

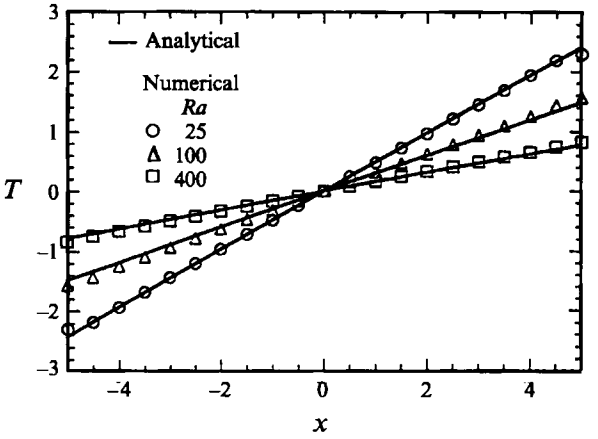

FIGURE 11. Horizontal temperature variation at the mid-height of the cavity compared with numerical results at $x = 0$.

values of the streamfunction (the values of $\psi(0, 0.5)$ in the numerical results) are shown as a function of *Ra*. Again the analytical and numerical results agree well over a wide range of the Rayleigh number. It is found that the value of ψ_{max} is less sensitive to grid refinement than the value of *Nu* in the numerical calculation; poor resolution in the numerical computation always leads to smaller values of *Nu*, but larger values for ψ_{max}, a trend easily observed in table 2.

Another physical quantity of interest is the horizontal temperature gradient *S* defined by (24). From (28), *S* decreases as $Ra^{-1/2}$ for large values of *Ra*; this trend is evident in figure 10(*c*), wherein the numerical solutions at $x = 0$ are also plotted together with the results of (28), and indicate favourable agreement. In addition, figure 11 shows the horizontal temperature variation at the mid-height of the cavity for three different values of *Ra*; it is perhaps rather surprising to see that the linear temperature profile in the *x*-direction persists even near the left and right end regions.

4.4. *Bifurcation from steady unicellular to oscillatory convection*

As predicted by the stability analysis of §3.3 for infinite aspect ratio, when the Rayleigh number is increased unicellular steady convection eventually becomes unstable. Two-dimensional linear stability analysis applied to the analytical solution for the fully developed regime indicates a critical Rayleigh number just in excess of 506, and that transition occurs via a Hopf bifurcation with onset oscillation frequency $f_{cr} = 22.1$ in diffusion time. Numerical computations indicate that the critical Rayleigh number depends on the geometric aspect ratio of the cavity, whose sidewalls ensure that unicellular flow is stable for values of *Ra* somewhat in excess of 506; in figure 12, for example, we show the isotherms and streamlines during a single period of oscillation at $Ra = 650$ for $A = 8$. In this series of plots we show the temporal deviations of the streamfunction and the temperature from their time-averaged mean values. It is seen that, along the horizontal walls, six or seven pairs of vortex-like flows are formed which subsequently move downstream with the main circulation. The pairs of vortices are obviously caused by periodic temperature variations at the horizontal walls. For the entire cavity, the spatial period is roughly 1.32 in dimensionless length, which compares well with the value 1.48 as determined by the critical wavenumber k_{cr} at the onset of oscillation for the case $A \to \infty, l = 0$. Furthermore, when such a pair of vortices impinges on the vertical sidewalls, and thereby changes its direction of motion, the flow

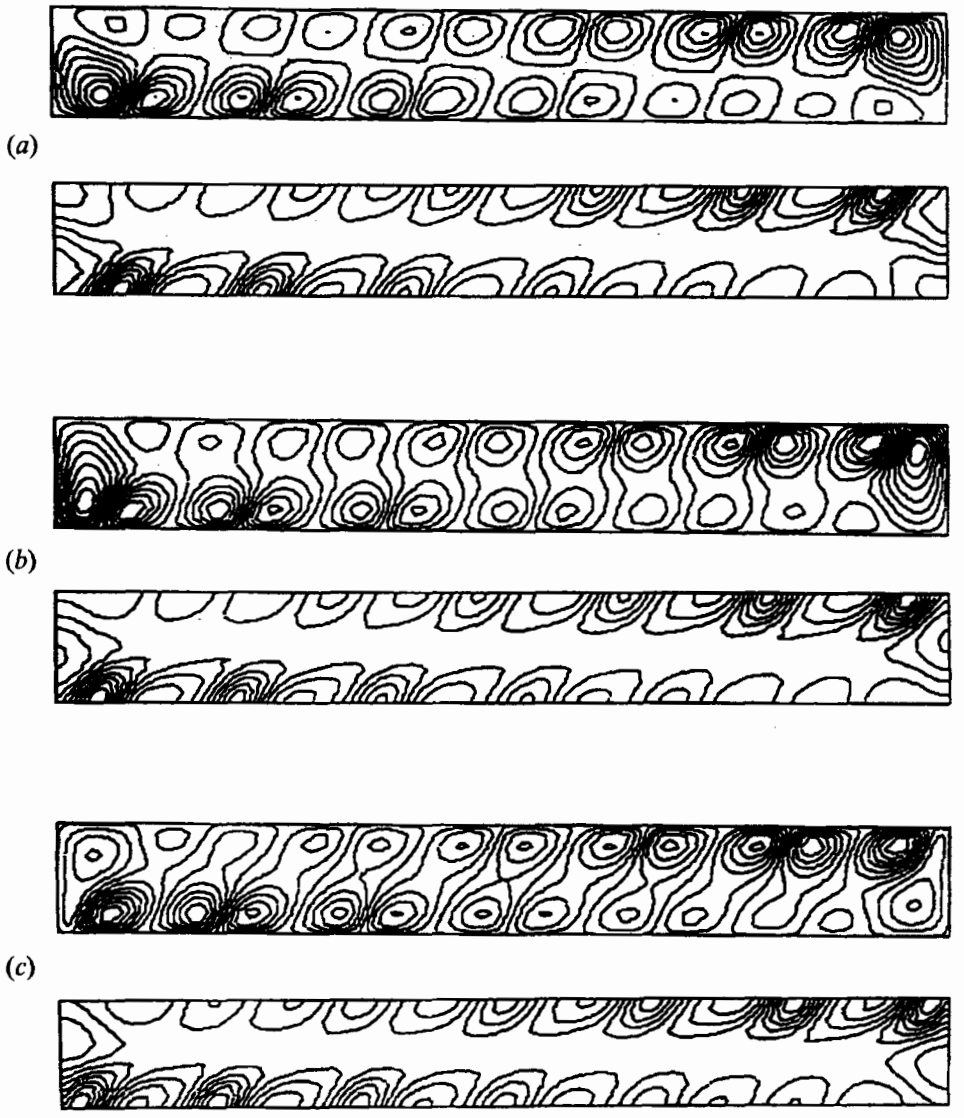

FIGURE 12(*a–c*). For caption see facing page.

strength within the pair diminishes. As for the observed oscillation in Nusselt number, this is attributable to the horizontal movement of a pair of temperature disturbances of unequal strength, which are responsible for alternate small and large amplitudes in the course of a single period at a fixed x-location.

The oscillatory flows obtained in the present numerical study were, for the most part, simply periodic for Ra smaller than 800; however, exceptions, where a small-amplitude oscillation with a higher harmonic frequency was superimposed onto the leading harmonic oscillation, were also observed. Such a case is shown in figure 13(*a*) which shows the Nusselt number variation in time and its spectral power curve near the onset of oscillation ($Ra = 650, A = 8$); the latter, consisting of peaks at $f = 22.7$ and its harmonics, quantifies the oscillation. Similarly the Nusselt number variation with time at $Ra = 750$ near the onset of oscillation for $A = 4$ and its spectral power curve are shown in figure 13(*b*). The dependency of Ra_{cr} on aspect ratio, evidently nonlinear, is

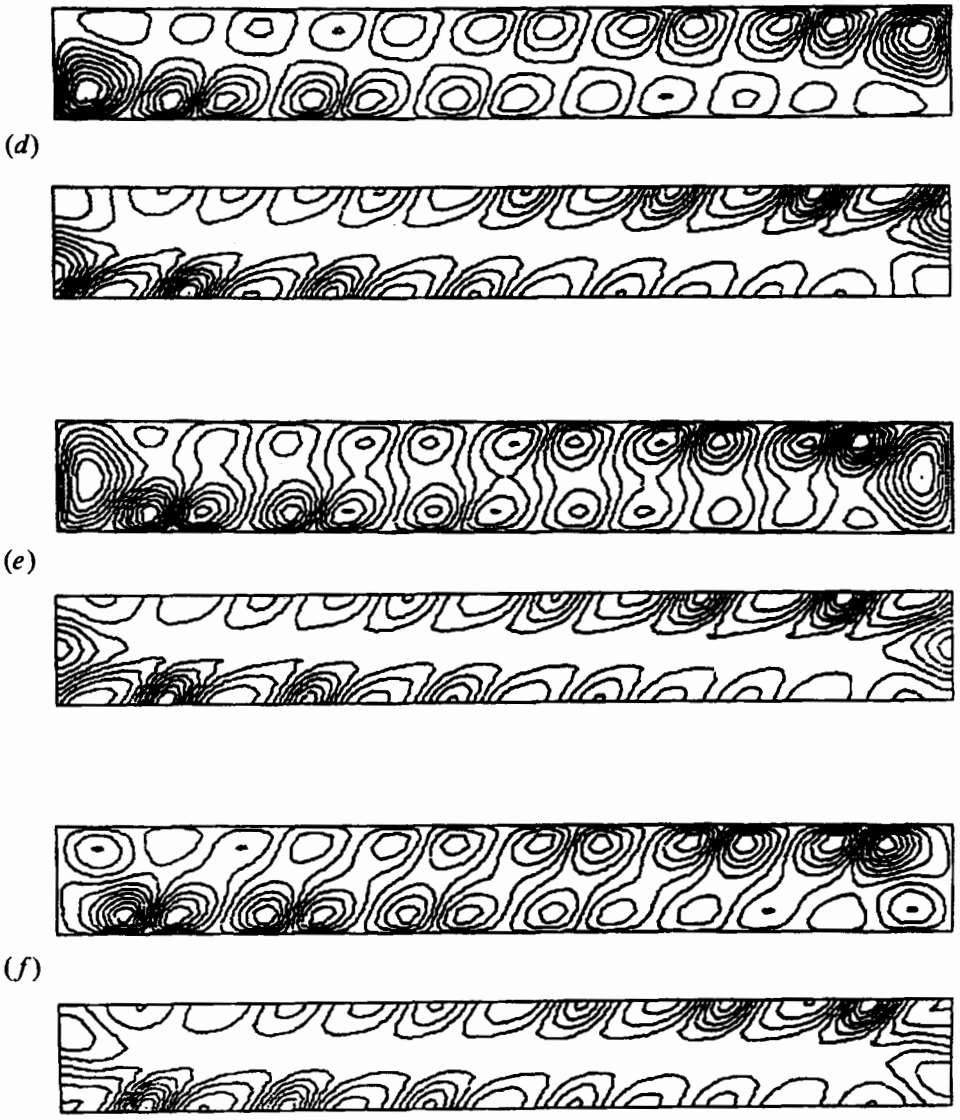

FIGURE 12. Temporal behaviour of the deviation of isotherms and streamlines from the time-averaged mean value of the single-cell solution at $Ra = 650$ during a single period of oscillation ($\Delta\theta = 3.6 \times 10^{-3}, \Delta\psi \approx 1, \psi_{max} \approx 10$). The time interval between successive figures is $\Delta t = 7.25 \times 10^{-3}$.

further elaborated in figure 14(*a*). Although it proved difficult to pin down exactly the critical Rayleigh for a given aspect ratio, it was observed to lie between 630 and 650 for $A = 8$, increasing to somewhere between 730 and 750 for $A = 4$. It would therefore seem plausible to suggest, in the absence of computations for higher aspect ratios, that Ra_{cr} should approach the value 506 as the aspect ratio is increased.

Similarly, as shown in figure 14(*b*), the frequency at the onset of oscillation depends on the aspect ratio; furthermore, it is observed that the oscillation frequency increases with Rayleigh number, a trend which qualitatively agrees with the evolution of convection due to constant-temperature heating. In that case, a boundary-layer instability causes oscillatory flow, and a boundary-layer thinning process results in a frequency increase; in the present case, however, it is not so obvious from the isotherms

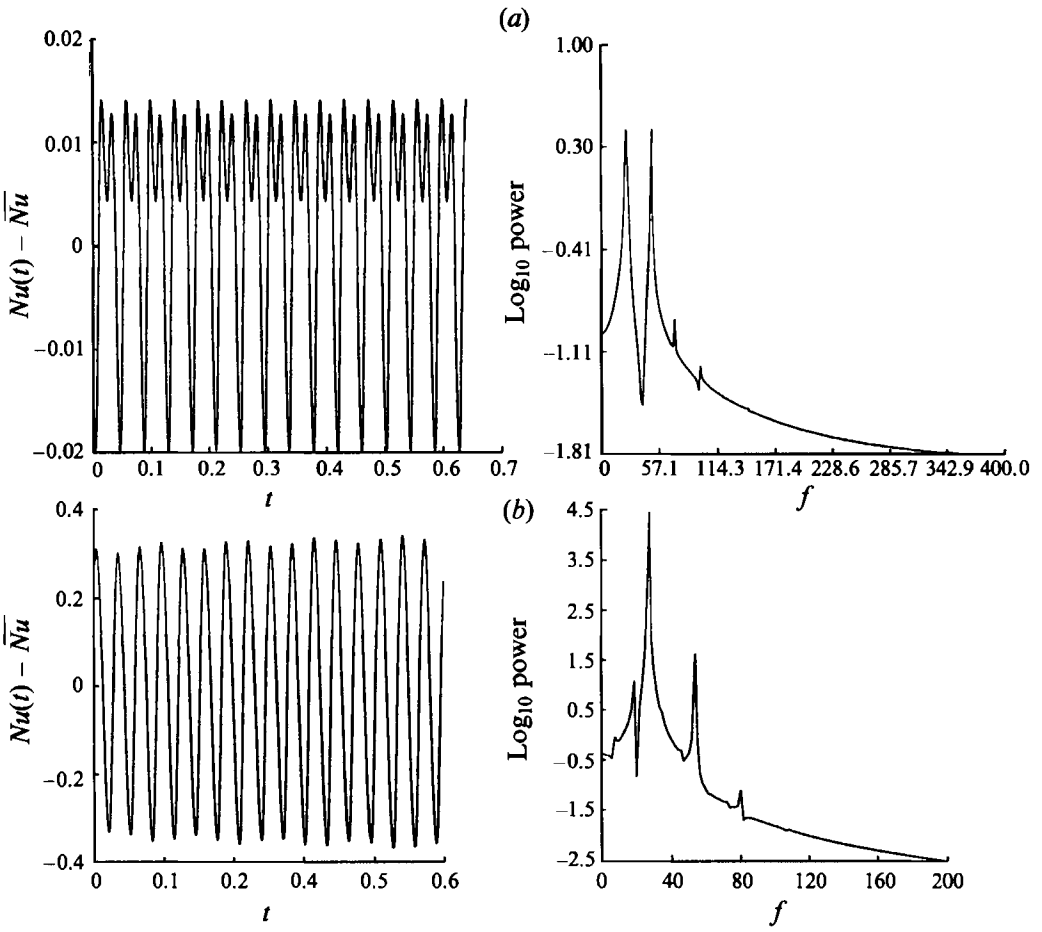

FIGURE 13. Oscillation of Nusselt number at $x = 0$ and its spectral power curve near criticality: (*a*) $Ra = 650$, $A = 8$; (*b*) $Ra = 750$, $A = 4$.

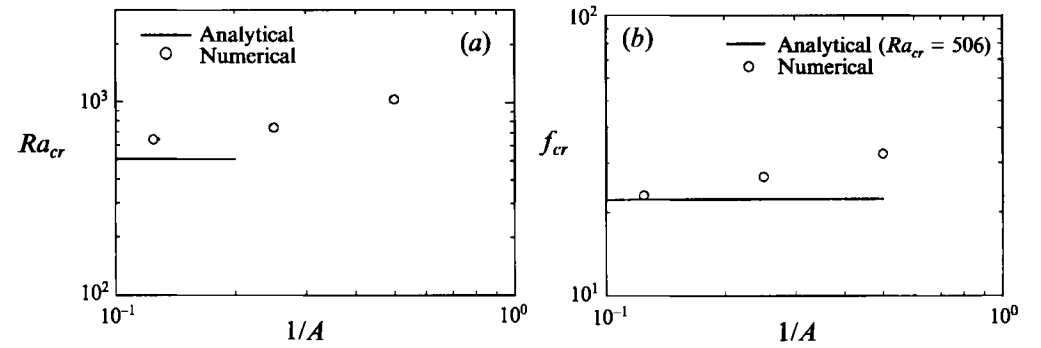

FIGURE 14. Critical Rayleigh number (*a*) and frequency at onset of oscillation (*b*) as a function of inverse aspect ratio.

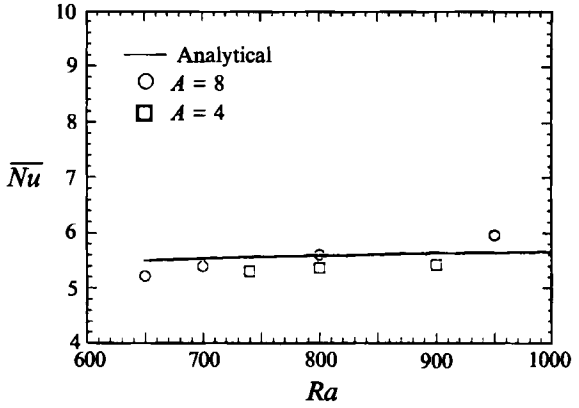

FIGURE 15. Time-averaged Nusselt number against Rayleigh number in an oscillatory regime.

and the streamlines whether or not a boundary-layer instability is responsible for the onset of oscillation. Nonetheless, there is no doubt that there are two competing mechanisms: the horizontal temperature gradient that drives the counterflow, and a vertical temperature gradient, which has the potential to destabilize it. In fact, examining the analytical solution for the temperature, it is not difficult to show that the vertical temperature gradient in the distance between either the top or bottom boundary and the first elbow (for instance, see figure 9*a*), increases with Ra, whereas the horizontal temperature gradient decreases with Ra. In the present problem, therefore, the effect of the vertical temperature gradient eventually overshadows the horizontal gradient, and thus leads to instability. It should be noted that this is exactly the situation discussed by Weber (1974) and Nield (1991); the latter has also pointed out the possibility of an oscillatory instability when the vertical Rayleigh number becomes sufficiently large. Finally, we present in figure 15 the time-averaged Nusselt number $\overline{Nu}$ as a function of Ra for two different aspect ratios; for these, the flow was unicellular for the values of Ra presented, and hence agreement with the analytical results for the fully developed flow is good.

5. Conclusion

An analytical and numerical study has been presented for the two-dimensional flow problem arising when a fluid-saturated porous cavity with a small aspect ratio (a shallow rectangle) is heated from below and cooled from above by a constant flux. It has been shown that a unicellular flow is stable up to a critical value of Ra, beyond which oscillatory convection sets in. Based on a fully developed counterflow assumption, an analytical solution for the velocity and temperature fields was developed, and the stability of this base solution was analysed. The linear stability analysis predicts that the base solution is stable to transverse disturbances up to $Ra_{cr} = 506.07$, at which point there is a Hopf bifurcation with critical oscillation frequency $f_{cr} = 22.1$ in diffusion time. The flow proves to be more unstable to longitudinal disturbances: an exchange of stability occurs for $Ra_{cr} \approx 311.53$ and critical wavenumber zero. For the two-dimensional case, extensive numerical computations have been carried out in order to complement the analysis; the Rayleigh number range studied in the numerical computations was $25 \leqslant Ra \leqslant 1050$, with aspect ratio A between 2 and 10. When steady unicellular convection exists, the simple

analytical solution predicts accurately the results of the full numerical solution; the physical quantities compared between the two were the temperature and velocity profiles in the vertical direction and the temperature gradient in the horizontal direction, although the analytical solution was not strictly speaking valid at the extreme left and right end regions.

The critical Rayleigh number for a Hopf bifurcation in the full numerical solutions shows some dependency on the cavity aspect ratio; for $A = 4$, the critical value for the onset of oscillation was around $Ra = 740$, whereas for $A = 8$ it was about $Ra = 640$. The oscillation frequency at criticality, f_{cr}, was also found to depend on the aspect ratio, although the value for $A = 8, f_{cr} = 22.7$, agreed well with the result obtained by the stability analysis.

Reiterating therefore, a fully developed counterflow can be induced when the top and bottom boundaries are subject to a constant-flux condition; this steady unicellular convective flow can exist for arbitrary aspect ratio up to a critical Rayleigh number which is slightly more than forty times greater than that for the onset of convection. This finding differs greatly from the flow observed when a shallow cavity is subject to constant-temperature heating from below, where multi-cellular convection is the preferred mode for aspect ratio in excess of $\sqrt{2}$.

The authors would like to acknowledge the constructive criticisms made by the referees during the preparation of this paper.

REFERENCES

AIDUN, C. K. & STEEN, P. H. 1987 Transition to oscillatory heat transfer in a fluid saturated porous medium. *J. Thermophys. Heat Transfer* **1**, 268–273.

ALAVYOON, F. 1992 The effects of porous separators on free convection and mass transfer in electrochemical systems – application to recharging lead-acid cells. In *Heat and Mass Transfer in Porous Media* (ed. M. Quintard & M. Todorović), pp. 349–379. Elsevier.

ALAVYOON, F. 1993 On natural convection in vertical porous enclosures due to prescribed fluxes of heat and mass at the vertical boundaries. *Intl J. Heat Mass Transfer* **36**, 2479–2498.

BARK, F. H., ALAVYOON, F. & DAHLKILD, A. A. 1992 On unsteady free convection in vertical slots due to prescribed fluxes of heat and mass at the vertical walls. *J. Fluid Mech.* **235**, 665–689.

BEJAN, A. 1983 The boundary layer regime in a porous layer with uniform heat flux from the side. *Intl J. Heat Mass Transfer* **26**, 1339–1346.

CALTAGIRONE, J. P. 1975 Thermoconvective instabilities in a horizontal porous layer. *J. Fluid Mech.* **72**, 268–287.

GARY, J. & KASSOY, D. R. 1981 Computation of steady and oscillatory convection in saturated porous media. *J. Comput. Phys.* **40**, 120–142.

HORNE, R. N. & O'SULLIVAN, M. J. 1974 Oscillatory convection in a porous medium heated from below. *J. Fluid Mech.* **66**, 339–352.

KASSOY, D. R. & COTTE, B. 1985 The effects of sidewall heat loss on convection in a saturated porous vertical slab. *J. Fluid Mech.* **152**, 361–378.

KIMURA, S. & POP, I. 1992 Conjugate natural convection between horizontal concentric cylinders filled with porous medium. *Wärme- und Stoffübertr.* **27**, 85–91.

KIMURA, S., SCHUBERT, G. & STRAUSS, J. M. 1986 Route to chaos in porous-medium thermal convection. *J. Fluid Mech.* **166**, 305–324.

KIMURA, S., SCHUBERT, G. & STRAUS, J. M. 1989 Time-dependent convection in a fluid-saturated porous cube heated from below. *J. Fluid Mech.* **207**, 153–189.

LOWELL, R. P. & SHYU, C. T. 1978 On the onset of convection in a water-saturated porous box: effect of conducting walls. *Lett. Heat Mass Transfer* **5**, 371–378.

MURPHY, H. D. 1979 Convective instabilities in vertical fractures and faults. *J. Geophys. Res.* **84**, 6121–6130.

NIELD, D. A. 1968 Onset of thermohaline convection in a porous medium. *Water Resources Res.* **4**, 553–560.

NIELD, D. A. 1991 Convection in a porous medium with inclined temperature gradient. *Intl J. Heat Mass Transfer* **34**, 87–92.

PATANKAR, S. V. 1980 *Numerical Heat Transfer and Fluid Flow*. Hemisphere.

RILEY, D. S. & WINTERS, K. H. 1989 Modal exchange mechanisms in Lapwood convection. *J. Fluid Mech.* **204**, 325–358.

RILEY, D. S. & WINTERS, K. H. 1991 Time periodic convection in porous media: the evolution of Hopf bifurcations with aspect ratio. *J. Fluid Mech.* **223**, 457–474.

SCHUBERT, G. & STRAUS, J. M. 1979 Three-dimensional and multi-cellular steady and unsteady convection in fluid-saturated porous media at high Rayleigh numbers. *J. Fluid Mech.* **94**, 25–36.

SCHUBERT, G. & STRAUS, J. M. 1982 Transitions in time-dependent thermal convection in fluid-saturated porous media. *J. Fluid Mech.* **121**, 301–313.

SEN, M., VASSEUR, P. & ROBILLARD, L. 1987 Multiple steady states for unicellular natural convection in an inclined porous layer. *Intl J. Heat Mass Transfer* **30**, 2097–2113.

STEEN, P. H. 1983 Pattern selection for finite-amplitude convection states in boxes of porous media. *J. Fluid Mech.* **136**, 219–242.

SUTTON, F. 1970 Onset of convection in a porous channel with net through flow. *Phys. Fluids* **13**, 1931–1934.

VASSEUR, P., SATISH, M. G. & ROBILLARD, L. 1987 Natural convection in a thin inclined porous layer exposed to a constant heat flux. *Intl J. Heat Mass Transfer* **30**, 537–549.

WANG, M., KASSOY, D. R. & WEIDMAN, P. D. 1987 Onset of convection in a vertical slab of porous media between two impermeable conducting blocks. *Intl J. Heat Mass Transfer* **30**, 1331–1341.

WEBER, J. E. 1974 Convection in a porous medium with horizontal and vertical temperature gradients. *Intl J. Heat Mass Transfer* **17**, 241–248.

WEIDMAN, P. D. & KASSOY, D. R. 1986 The influence of side wall heat transfer on convection in a confined saturated porous medium. *Phys. Fluids* **29**, 349–355.